Thermochemistry for Hydrocarbon Intermediates Chemisorbed on Metal Surfaces: $CH_{n-m}(CH_3)_m$ with $n = 1, 2, 3$ and $m \leq n$ on Pt, Ir, Os, Pd, Rh, and Ru

Jeremy Kua, Francesco Faglioni, and William A. Goddard, III*

Contribution from the Materials and Process Simulation Center, Beckman Institute (139-74), Division of Chemistry and Chemical Engineering, California Institute of Technology, Pasadena, California 91125

Received September 14, 1999

Abstract: To provide insight and understanding of the thermochemistry underlying hydrocarbon rearrangements on transition metal surfaces, we report systematic studies of hydrocarbon radicals chemisorbed on metal clusters representing the closest packed surfaces of the six second and third row group VIII transition metals. Using first principles quantum mechanics [nonlocal density functional theory with exact HF exchange (B3LYP)], we find that (i) $CH_{3-m}(CH_3)_m$ forms one bond to the surface, preferring the on-top site (η^1), (ii) $CH_{2-m}(CH_3)_m$ forms two bonds to the surface, preferring the bridge site (η^2), and (iii) $CH_{1-m}(CH_3)_m$ forms three bonds to the surface, preferring the 3-fold site (η^3). For all six metals, the adiabatic bond energy is nearly proportional to the number of bonds to the surface, but there are dramatic decreases in the bond energy with successive methyl substitution. Thus from CH_3 to CH_2CH_3, $CH(CH_3)_2$, and $C(CH_3)_3$, the binding energy decreases by 6, 14, and 23 kcal/mol, respectively (out of ∼50). From CH_2 to $CHCH_3$ and $C(CH_3)_2$, the binding energy decreases by 8 and 22 kcal/mol, respectively (out of ∼100). These decreases due to methyl substitution can be understood in terms of steric repulsion with the electrons of the metal surface. For CH to $C(CH_3)$, the bond energy decreases by 13 kcal/mol (out of ∼160), which is due to electronic promotion energies. These results are cast in terms of a thermochemical group additivity framework for hydrocarbons on metal surfaces similar to the Benson scheme so useful for gas-phase hydrocarbons. This is used to predict the chemisorption energies of more complex adsorbates.

1. Introduction

Hydrocarbon reactions and rearrangements catalyzed by transition metal surfaces underlie the chemical processes at the core of the petrochemical and polymer industries. These include[1] (1) hydrogenation of unsaturated hydrocarbons, (2) double-bond isomerization of olefins, (3) dehydrogenation and dehydroisomerization to aromatics, (4) isomerization of alkanes, (5) dehydrocyclization, and (6) hydrogenolysis.

The fundamental reactions in these processes involve the breaking and forming of C−C, C−H, M−C, and M−H bonds on catalysts usually involving the late transition metals (group VIII), particularly Pt, Pd, and Ni. Yet, despite intensive experimental study there remain major gaps in our understanding of mechanism and energetics of these essential industrial processes.

Although molecular orbital and valence bond theories have helped explain the nature of reactivity in organic and single metal center organometallic reactions, there has been little progress in understanding how the orbitals control reactions on metal surfaces. Thus the extensive experimental work on skeletal isomerization on platinum[2] provided valuable information about cyclic and bond-shift mechanisms but little understanding of the role of the metal. Surface science experiments helped characterize some intermediates in chemisorption and reactions on metal surfaces.[3−5] However, little or nothing is known about most potential intermediates and, with the exception of work by Carter,[6,7] there is little in the way of thermochemical concepts about chemisorbed intermediates.

To lay the foundation for developing both the thermochemical data needed for design and control process and the mechanistic information useful for chemical reasoning about reactions on metals surfaces, we carried out systematic calculations on the structures and energetics for $CH_{n-m}(CH_3)_m$ fragments with $n = 1,2,3$ and $m \leq n$ at on-top, bridging, and cap sites of the six second and third row group VIII transition metals (Pt, Ir, Os, Pd, Rh, and Ru). Such systematic studies allow us to examine group additivity and substituent effects for prototypical hydrocarbon intermediates chemisorbed on a range of metal surfaces. This allows us to estimate the steric and electronic contributions affecting binding and reactivity. We expect that such semiquantitative concepts could become a powerful tool in understanding and predicting the reactions of larger and more complex hydrocarbons on metal surfaces. We would hope that thermochemical concepts on the stability of various intermediates would lead to the predictive power contained in Benson group additivities so useful in understanding mechanisms of organic reactions.[8,9]

* To whom correspondence should be addressed (E-mail: wag@wag.caltech.edu).

(1) Davis, S. M.; Somorjai, G. A. *The Chemical Physics of Solid Surfaces and Heterogeneous Catalysis*, King, D. A., Woodruff, D. P., Eds.; Elsevier: Amsterdam, 1982; Vol. 4, pp 217−298.

(2) Gault, F. G. *Adv. Catal.* **1981**, *30*, 1.

(3) Albert, M. R.; Yates, J. T., Jr. *The Surface Scientists Guide to Organometallic Chemistry*; American Chemical Society: Washington, 1987.

(4) Somorjai, G. A. *Introduction to surface chemistry and catalysis*; Wiley: New York, 1994.

(5) Zaera, F. *Chem. Rev.* **1995**, *95*, 2561.

(6) Koel, B. E.; Blank, D. A.; Carter, E. A. *J. Mol. Cat A-CHEM* **1998**, *131*, 39.

(7) Carter, E. A.; Koel, B. E. *Surf. Sci.* **1990**, *226*, 339.

10.1021/ja993336l CCC: $19.00
Published on Web 02/24/2000

Table 1. Spin State and Total Energies (hartree) for CH_x/M_8 from QM (B3LYP DFT)

M	CH_3	CH_2	CH	C	none
			Total Energy (hartree)		
Pt	−993.184 32	−992.575 07	−992.002 22	−991.344 24	−953.257 26
Ir	−877.328 44	−876.719 14	−876.142 72	−875.494 44	−837.406 01
Os	−767.925 30	−767.314 25	−766.737 10	−766.096 68	−728.009 41
Pd	−1053.906 74	−1053.296 31	−1052.710 78	−1052.082 02	−1013.985 67
Rh	−915.907 60	−915.295 00	−914.715 93	−914.078 60	−875.987 23
Ru	−790.740 33	−790.129 99	−789.545 08	−788.908 09	−750.834 65
			Total Spin		
Pt	5/2	2	5/2	3	3
Ir	13/2	6	11/2	7	8
Os	19/2	10	19/2	10	10
Pd	3/2	2	3/2	2	1
Rh	13/2	6	11/2	6	7
Ru	21/2	10	21/2	11	11

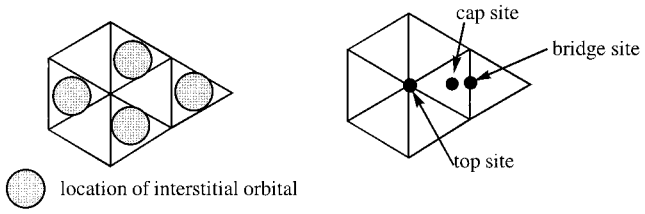

Figure 1. M_8 cluster model for closed-packed surfaces of group VIII metals.

To study such an enormous range of systems at a consistent level of accuracy, we have modeled the metal surface as a closest packed but planar cluster with eight metal atoms as shown in Figure 1. This is based on the interstitial electron model (IEM) developed recently from studies of the bonding in platinum clusters.[10] We previously reported studies using this cluster to examine all CH_x and C_2H_x intermediates on platinum[11] and a variety of CH_xO and OH_x intermediates important in direct methanol fuel cell catalysis on Pt, Ir, Os, Pd, Rh, and Ru.[12] These calculations lead to geometries and energetics in good agreement with available experimental results on Pt(111) surfaces, suggesting that it is an accurate model.

In section 2 we consider the chemisorption of various CH_x species at various sites for the various metals. These results are used to lay out many of the ideas. section 3 then considers various substituents $CH_{n-m}(CH_3)_m$ for $n = 1, 2, 3$ and $m \leq n$. These results are used to extract steric effects and other quantities concerning the chemisorbed species. Section 4 then uses these results to extract group additivities and applies them to predicting such species as chemisorbed di-σ ethylene and di-σ cyclohexene. A recipe for how to apply the group additivity derived in this paper is provided at the end of section 4. The concluding summary is in section 5 while section 6 summarizes the computational details.

2. Chemistry of Chemisorbed CH_x

2.1. Structures and Energetics. To examine the preference of hydrocarbons for various sites on the closest packed surfaces of the six metals, we calculated the optimum geometries of CH_3, CH_2, and CH in the top, bridge, and cap (hollow fcc) sites. The optimized structures are shown in Figure 2. Table 1 lists the total energy and spin states, Table 2 lists the binding energies, and Table 3 lists the M−C bond distances of all these species.

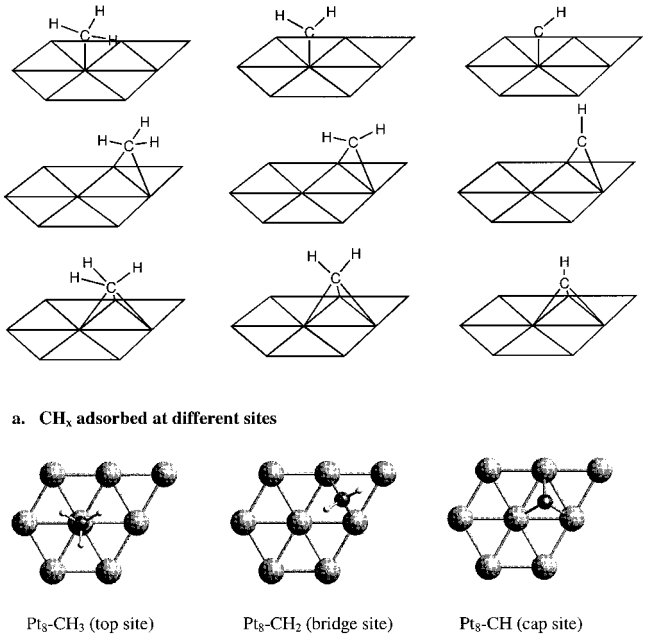

Figure 2. CH_x adsorbed on M_8.

Table 2. Adiabatic Binding Energies (kcal/mol) for CH_x/M_8 Clusters[a]

	CH_3	CH_2	CH		CH_3	CH_2	CH
		Pt				**Pd**	
top	**53.77**	78.07	80.93	top	**50.01**	70.94	85.35
bridge	26.87	**104.28**	149.37	bridge	41.54	**99.79**	137.85
cap	22.52	80.54	**166.60**	cap	32.41	91.53	**154.14**
		Ir				**Rh**	
top	**50.87**	78.26	82.96	top	**49.58**	83.32	91.89
bridge	24.72	**101.34**	152.80	bridge	35.04	**97.98**	137.97
cap	17.36	77.20	**161.42**	cap	25.27	84.21	**151.43**
		Os				**Ru**	
top	**46.76**	74.81	94.19	top	**40.36**	65.84	94.15
bridge	17.59	**96.14**	142.99	bridge	25.20	**90.18**	132.78
cap	14.67	78.70	**155.76**	cap	20.54	77.07	**144.93**

[a] The binding energies for the most stable sites form the diagonal and are highlighted in bold.

(The values for CH_x/Pt_8 were obtained from ref 11.) The binding energies and M−C bond distances for the most stable sites form the diagonal and are highlighted in bold.

For each fragment on all six metals, the preferred binding site is the one allowing carbon to form four σ bonds. Thus, the most stable binding site for CH_3 is the top site (η^1 bound), CH_2 the bridge site (η^2 bound), and CH the cap site (η^3 bound).

(8) Benson, S. W. *Thermochemical Kinetics*; Wiley: New York, 1968.
(9) Cohen, N.; Benson, S. W. *Chem. Rev.* **1993**, *93*, 2419.
(10) Kua, J.; Goddard, W. A., III *J. Phys. Chem. B* **1998**, *102*, 9492.
(11) Kua, J.; Goddard, W. A., III *J. Phys. Chem. B* **1998**, *102*, 9499.
(12) Kua, J.; Goddard, W. A., III *J. Am. Chem. Soc.* **1999**, *121*, 10928.

Table 3. Pt−C Bond Lengths (in Å) of CH_x/M_8 Clusters[a]

	CH_3	CH_2	CH		CH_3	CH_2	CH
		Pt				**Pd**	
top	**2.07**	1.84	1.88	top	**2.01**	1.83	1.77
bridge	2.41	**2.01**	1.86	bridge	2.28	1.98	1.85
cap	2.63	2.11	**1.95**	cap	2.37	2.06	**1.93**
		Ir				**Rh**	
top	**2.09**	1.84	1.69	top	**2.04**	1.82	1.79
bridge	2.31	**2.06**	1.88	bridge	2.26	**2.01**	1.87
cap	2.65	2.11	**1.98**	cap	2.35	2.05	**1.95**
		Os				**Ru**	
top	**2.12**	1.87	1.71	top	**2.10**	1.85	1.78
bridge	2.40	**2.08**	1.92	bridge	2.32	**2.03**	1.91
cap	2.44	2.17	**2.02**	cap	2.45	2.12	**1.98**

[a] The M−C bond distances for the most stable sites form the diagonal and are highlighted in bold.

Table 4. Average M−C σ Bond Strength (in kcal/mol)

metal	CH_3	CH_2	CH
Pt	53.8	52.1	55.5
Ir	50.9	50.7	53.8
Os	46.7	48.1	51.9
Pd	50.0	49.9	51.4
Rh	49.6	49.0	52.1
Ru	40.4	45.1	48.3

The adiabatic binding energies are also roughly additive, i.e., the total bond energy to the surface is roughly 50 kcal/mol times the number of M−C bonds. Table 4 lists the average M−C σ bond strength based on the adiabatic binding energy. In nearly every case, the average M−C bonds are within 3 kcal/mol of each other. Exceptions are that CH_3/Os_8 is 5.2 kcal/mol weaker than the average from CH/Os_8, and CH_3/Ru_8 is 4.7 and 7.9 kcal/mol weaker than the average from CH_2/Ru_8 and CH/Ru_8, respectively.

For the fcc metals (Pt, Pd, Ir, Rh), the M−C bond of CH_3/M_8 is slightly stronger than the average M−C bond of CH_2/M_8, but this is reversed for the hcp metals (Os, Ru). For all six metals, the most significant trend is that the average M−C bond strengths of CH/M_8 are all ∼3 kcal/mol higher than the average M−C bond strengths of CH_2/M_8, suggesting that there may be added stability associated with the 3-fold site.

The adiabatic binding energies *increase across the row* (Os < Ir < Pt for the third row; Ru < Rh < Pd for the second row) and *down the columns* (Pd < Pt; Rh < Ir; Ru < Os) of the periodic table. The anomalous case is CH/Pd_8, which has a slightly weaker binding energy than CH/Rh_8 (difference of 2.7 kcal/mol). For CH_2 and CH_3, the bond to Pd is slightly stronger than to Rh (differences are 0.4 and 1.8 kcal/mol, respectively). This arises from the strong stabilization for Pd atom of the d^{10} configuration over the s^1d^9 configuration, which causes Pd to not follow the IEM rules as well as the other five metals. The Pt−C bond is the strongest (∼54 kcal/mol) and Ru−C is the weakest (∼45 kcal/mol).

The M−C bond lengths decrease across the row and increase down the column, reflecting the normal changes in atomic size.

2.2. QM Heats of Formation. To study the energetics of hydrogenation/dehydrogenation reactions involving chemisorbed CH_x species, we converted our calculated energies into heats of formation for each chemisorbed species. We chose the following as reference compounds: the M_8 metal cluster ($\Delta H_f = 0$), gas-phase CH_4 ($\Delta H_f = -17.9$ kcal/mol), and gas-phase H_2 ($\Delta H_f = 0$).

A thorough example was worked out for CH_x/Pt_8 (ref 11), and we apply this same method to CH_x/M_8 of all the metals studied here.

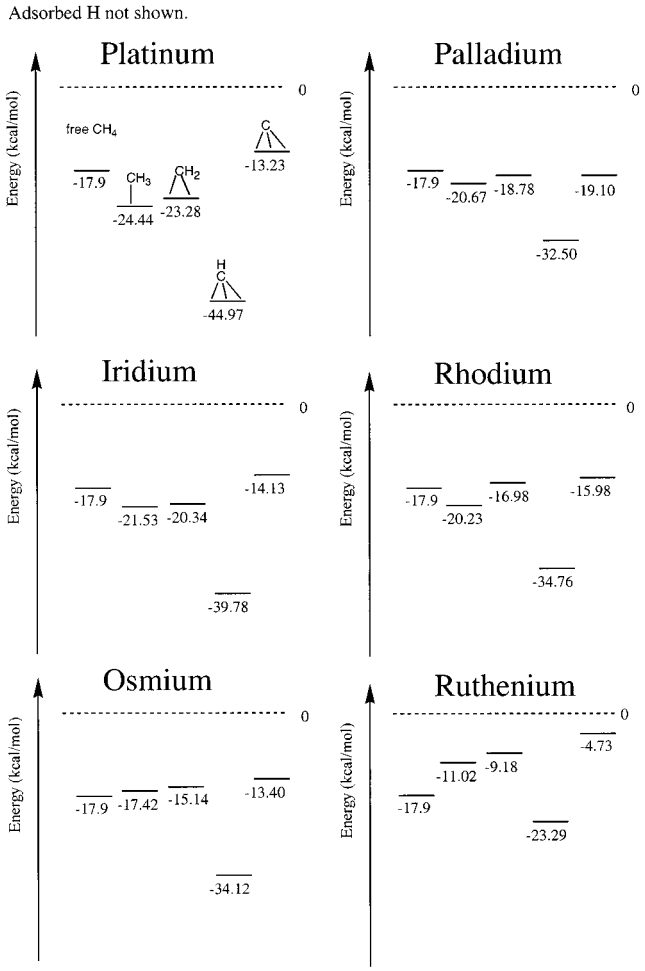

Figure 3. Heats of formation of CH_x/M_8.

On the basis of HREELS experiments, it is known that H atom prefers binding to the cap site on Pt(111).[13] We find the binding energy for H in the cap site to be 67.2 kcal/mol. Using the same method, the calculated desorption enthalpy to obtain gas-phase H_2 is 11.38 kcal/mol per adsorbed H.[11] This compares with 10.4 kcal/mol obtained from thermal desorption spectroscopy (TDS).[14] Similar experimental techniques yield desorption enthalpies (per adsorbed H) of 12.6 kcal/mol for Ir(111),[15] 10.6 kcal/mol for Pd(111),[16] 10.1 kcal/mol for Rh(111),[17] and 9.5 kcal/mol for Ru(0001).[18] To simplify the comparison of bond energies of different adsorbates on these various metals, we used the same value of −11.38 kcal/mol (calculated for Pt) for all the metals.

The heats of formation for the most stable CH_x species are shown in Figure 3 for all six metals. The total energies and spin states are given in Table 1. We find the following trends:

(1) $(CH)_{ads}$ is the thermodynamic sink for all six metals.

(2) The first dehydrogenation to form $(CH_3)_{ads} + H_{ads}$ from gas-phase methane is downhill for the fcc metals (Pt, Ir, Pd, Rh) and uphill for the hcp metals (Os, Ru).

(3) The second dehydrogenation step converting $(CH_3)_{ads}$ to $(CH_2)_{ads} + H_{ads}$ is slightly uphill for all six metals.

(13) Richter, L. J.; Ho, W. *Phys. Rev. B* **1987**, *36*, 9797.
(14) Christmann, K.; Ertl, G.; Pignet, T. *Surf. Sci.* **1976**, *54*, 365.
(15) Engstrom, J. R.; Tsai, W.; Weinberg, W. H. *J. Chem. Phys.* **1987**, *87*, 3104.
(16) Conrad, H.; Ertl, G.; Latta, E. E. *Surf. Sci.* **1974**, *41*, 435.
(17) Yates, J. T., Jr.; Thiel, P. A.; Weinberg, W. H. *Surf. Sci.* **1979**, *84*, 427.
(18) Feulner, R.; Menzel, D. *Surf. Sci.* **1985**, *154*, 465.

(4) The final dehydrogenation step to form adsorbed C is quite uphill for all six metals.

(5) Thermodynamically, Pt is the most favorable toward methane dehydrogenation while Ru is the least favorable.

For simplicity in comparing a large number of adsorbates on a number of metals and sites, we reference our calculated energetics for the minimized structures to experimental heats of formation of organics at room temperature and assign the naked metal cluster a heat of formation of zero. This provides an implicit first-order correction for zero point energy and changes in the enthalpy to room temperature to the calculated heats of formation, but is not rigorous. A more accurate method would be to calculate zero point energies and room temperature enthalpy changes directly for every cluster and molecule as a direct correction. This difference may lead to changes in the final heat of formation of a few kilocalories/mole. In section 6.4, we compare the implicit to explicit calculations for H/Pt_8. However, our interest here is to provide a simple method to predict the relative stability of a large number of adsorbates. Since these changes are expected to be nearly the same for adsorbates at the same site of the various metals, implying a constant correction to the current results, we choose to neglect these corrections herein. Section 4 contains examples of using such bond additivities to predict bond energies and heats of formation of various other chemisorbed molecules.

2.3. Comparison with Previous Experimental and Computational Studies. 2.3.1. Pt. There is kinetic and spectroscopic evidence for methyl, methylidene (CH_2), and methylidyne (CH) moieties on Pt(111).[19] However, neither the energetics nor the structures of CH_x species adsorbed on Pt(111) have been sufficiently characterized experimentally to provide a test of the calculations.

Low-energy electron irradiation of CH_4 on Pt(111) shows evidence of C−H bond cleavage to form chemisorbed methyl and chemisorbed hydrogen atoms.[20] Molecular beam surface scattering experiments find that the dissociative chemisorption of methane is enhanced by increasing both the translational energy of methane and the surface temperature.[21] Adsorbed methyl species has also been generated via gas-phase pyrolysis of azomethane.[22]

Microcalorimetric studies suggest that intrinsic Pt−C bond energies on Pt(111) are in the range of 54−64 kcal/mol,[23] in agreement with our calculations.

DFT (B3LYP) quantum calculations of CH_x on a Pt_{10} (6.3.1) trilayer cluster with a basis set similar to ours yielded results[24] in agreement with ours.[11] They find that CH_3 prefers an on-top site, CH_2 a bridge site, and CH a cap site (bond energy data was not provided). The cluster chosen for these calculations does not have the s^1d^9 configuration, and spin was not optimized.

CH_4 activation has also been studied on small clusters of Pt and Pd ranging from 1 to 3 atoms.[25,26] Essentially these clusters model edge sites rather than terraces of an extended metal and concentrate only on the first step of C−H activation.

Akinaga et al. used B3LYP density functional theory with small Pt clusters to study the photodissociation of methane on the Pt(111) surface.[27] Their study was motivated by the experimental work of Watanabe et al.[28] They find that the Rydberg-type first excited state of methane strongly interacts with Pt_N unoccupied states, resulting in a charge-transfer state that finally leads to the dissociation of methane. Their calculations indicate that the excitation energy to the Rydberg state of methane interacting with Pt decreases by ~3 eV compared to isolated methane. This is consistent with the experimental observation that irradiation with 193 nm photons of methane over Pt(111) surface leads to photodissociation.

Feng et al. computed CH_3, CH_2, and CH on small planar Pt clusters using DV-Xα methods (DFT but without gradient or exact exchange corrections) with similar results.[29] They find binding energies of 56.7, 93.4, and 149.2 kcal/mol to the top, bridge, and cap sites of Pt_7, Pt_{10}, and Pt_{12} planar clusters (chosen to match the symmetry of the adsorbate.) This compares to our values of 53.8, 104.3, and 166.6 kcal/mol, respectively.

2.3.2. Ir. A study of the dissociative chemisorption of methane on Ir(111) found two distinct pathways:[30] (i) a trapping-mediated pathway with a lower activation energy (12.6 kcal/mol) and (ii) a direct pathway with a higher activation energy (17.4 kcal/mol).

This study did not investigate subsequent CH_x adsorbed species on the Ir(111) surface.

2.3.3. Os. We know of no publications investigating CH_4 dissociation on Os(0001).

2.3.4. Pd. Paul and Sautet[31] calculated CH_x on Pd(111) using gradient-corrected DFT calculations on two- and three-layer slabs with periodic boundary conditions. The GGA PW91 functional was used for structural optimization and calculation of binding energies. The basis set was of double-ζ quality [a combination of Slater-type orbitals (STO) and natural atomic orbitals (NAO)] and includes an 18-electron effective core potential for Pd. The calculated coverage is 1/3 monolayer. The site preference is in agreement with our results: CH_3 on-top, CH_2 bridge, and CH cap. Their calculated binding energies of 39.4, 84.4, and 136.1 kcal/mol are respectively 10−18 kcal/mol lower than our values of 50.0, 99.8, and 154.1. Their Pd−C bond lengths of 2.05, 2.03, and 1.95 Å, respectively, are 0.02−0.05 Å larger than our values of 2.01, 1.98, and 1.93. The lower binding energies found in these slab calculations may arise from the difference between a full monolayer and the low coverage limit. Thus, in microcalorimetric studies, Yeo[23] found a 12 kcal/mol decrease in the heat of reaction of ethylene on Pt(111) as the coverage increased from zero concentration to 0.2 monolayers. Differences in basis set and density functionals might also account for a few kcal/mol of the discrepancy. In addition, it might be that cluster calculations would give a higher binding energy than a slab at very low coverage. Unfortunately, there does not yet seem to be a direct comparison between cluster and slab calculations using the same basis sets and density functionals.

2.3.5. Rh. Extended Huckel calculations using empirical two-body energy corrections (ASED-MO) on Rh(111)[32] lead to the

(19) Zaera, F. *Langmuir* **1991**, *7*, 1998.
(20) Alberas-Sloan, D. J.; White, J. M. *Surf. Sci.* **1996**, *365*, 212.
(21) Valden, M.; Xiang, N.; Pere, J.; Pessa, M. *Appl. Surf. Sci.* **1996**, *99*, 83.
(22) Fairbrother, H. D.; Peng, X. D.; Trenary, M.; Stair, P. C. *J. Chem. Soc., Faraday Trans.* **1995**, *91*, 3619.
(23) Yeo, Y. Y.; Stuck, A.; Wartnaby, C. E.; King, D. A. *Chem. Phys. Lett.* **1996**, *259*, 28. The 30−48 kcal/mol microcalorimetry measurements are interpreted as ethylene adsorption in the smaller range, converting to ethylidyne in the larger range.
(24) Watwe, R. M.; Speiewak, B. E.; Cortright, R. D.; Dumesic, J. A. *J. Catal.* **1998**, *180*, 184.
(25) Blomberg, M. R. A.; Siegbahn, P. E. M.; Svensson, M. *J. Phys. Chem.* **1992**, *96*, 5783.
(26) Cui, Q.; Musaev, D. G.; Morokuma, K. *J. Chem. Phys.* **1998**, *108*, 8418.
(27) Akinaga, Y.; Taketsugu, T.; Hirao, K. *J. Chem. Phys.* **1997**, *107*, 415.
(28) Watanabe, K.; Sawabe, K.; Matsumoto, Y. *Phys. Rev. Lett.* **1996**, *76*, 1751.
(29) Feng, K. A.; Lin, Z. D. *Appl. Surf. Sci.* **1993**, *72*, 139.
(30) Jachimowski, T. A.; Hagedorn, C. J.; Weinberg W. H. *Surf. Sci.* **1997**, *393*, 126.
(31) Paul, J.-F.; Sautet, P. *J. Phys. Chem. B* **1998**, *102*, 1578.

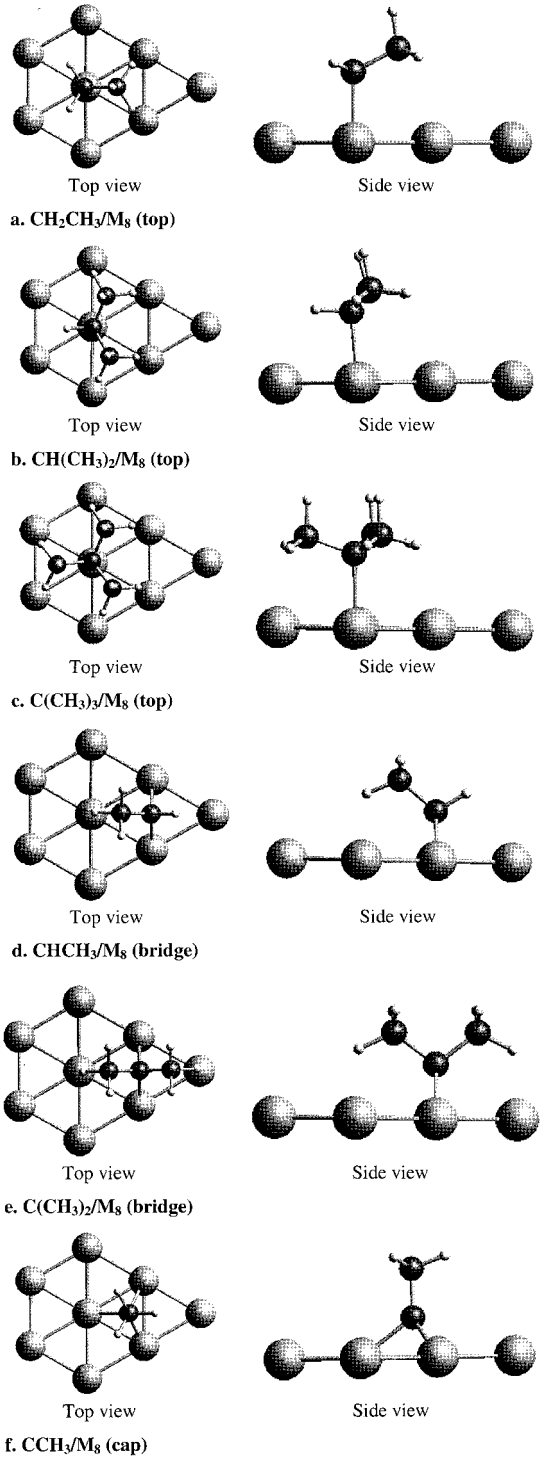

Figure 4. CR_x adsorbed on M_8.

same site preferences; we find: CH_3 on-top, CH_2 bridge, and CH cap. The binding energies of 68.0, 106.3, and 151.7 kcal/mol, respectively, are somewhat larger than our values of 49.6, 97.8, and 151.4, respectively.

2.3.6. Ru. On Ru(0001), HREELS experiments have identified a stable CH (methylidyne) species located in the cap site.[33] The assignment of the C−H peak comes from comparison to the $Ru_3(\mu_3\text{-}CH)(CO)_9$ organometallic complex.[34] On the basis of analogy to similar organometallic complexes of various metals, the HREELS results on Rh(111), Pd(111), and Pt(111) have been interpreted in terms of chemisorbed CH.[33] These observations are compatible with our calculations showing that CH is the most stable CH_x species on all of these surfaces.

(32) De Koster, A.; Van Santen, R. A. *J. Catal.* **1991**, *127*, 144.
(33) Wu, M.-C.; Goodman, D. W. *J. Am. Chem. Soc.* **1994**, *116*, 1364.
(34) Oxton, I. A. *Spectrochim. Acta A* **1982**, *38*, 181.

Table 5. Adiabatic Binding Energies of CR_x/M_8 (in kcal/mol)[a]

a. CR_3 Series

metal	CH_3	CH_2CH_3	$CH(CH_3)_2$	$C(CH_3)_3$
Pt	53.8	48.6 (−5.2)	41.1 (−12.7)	31.0 (−22.8)
Ir	50.9	46.0 (−4.9)	38.4 (−12.5)	26.1 (−24.8)
Os	46.7	39.4 (−7.3)	33.8 (−13.1)	25.8 (−20.9)
Pd	50.0	43.3 (−6.7)	33.9 (−16.1)	25.3 (−24.7)
Rh	49.6	43.7 (−5.9)	37.4 (−12.2)	28.8 (−20.8)
Ru	40.4	33.3 (−7.1)	25.3 (−15.1)	13.8 (−26.6)
average difference		(−6.2 ± 1.3)	(−13.6 ± 2.5)	(−23.4 ± 3.2)

b. CR_2 Series

metal	CH_2	$CHCH_3$	$C(CH_3)_2$
Pt	104.3	98.1 (−6.2)	84.8 (−19.5)
Ir	101.3	92.0 (−9.3)	78.0 (−23.3)
Os	96.1	86.8 (−9.3)	71.2 (−24.9)
Pd	99.8	92.1 (−6.7)	78.1 (−21.7)
Rh	98.0	88.6 (−9.4)	80.6 (−17.4)
Ru	90.2	81.9 (−8.3)	68.2 (−22.0)
average difference		(−8.2 ± 2.0)	(−21.5 ± 3.4)

c. CR series

metal	CH	CCH_3
Pt	166.6	154.7 (−11.9)
Ir	161.4	150.1 (−11.3)
Os	155.8	142.0 (−13.8)
Pd	154.1	142.8 (−11.3)
Rh	156.4	142.7 (−13.7)
Ru	144.9	130.9 (−14.0)
average difference		(−12.7 ± 1.4)

[a] Numbers in parentheses indicate the difference in binding energy with respect to CH_x.

3. Methyl Substitution on CR_x/M_8

3.1. Structures and Energetics. The general effect of successive methyl substitution is to decrease the adiabatic binding energy. The final substitution to form a "quaternary" carbon shows the largest decrease. The M−C bond lengths also increase with increasing substitution. This effect is very pronounced in the CR_3 series, less so in the CR_2 series, and not observable in the CR series. For the partially methylated species, there is some tilting of the adsorbed species due to sterics. For example, $CH(CH_3)_2$ tilts so that the two CH_3 groups move away from the surface while the H "group" moves toward the surface (C−C−Pt and H−C−Pt bond angles of 112° and 95°, respectively, compared to H−C−Pt bond angle in CH_3/Pt_8 of 106°). Structures are shown in Figure 4. Adiabatic binding energies are reported in Table 5, and corresponding M−C bond lengths are reported in Table 6. The ground spin states of CR_x/M_8 are the same as for CH_x/M_8 with the exception of CCH_3/Ir_8, where the ground spin state is $S = 13/2$ rather than 11/2.

3.1.1. CR_3 Series. For the series $CH_3 \rightarrow CH_2CH_3 \rightarrow CH(CH_3)_2 \rightarrow C(CH_3)_3$, the adiabatic binding energy decreases by an average (over all six metals) of 6.2, 13.6, and 23.4 kcal/mol compared to CH_3/M_8. This is very significant since the average M−C bond energy of CH_3/M_8 is only 48.6 kcal/mol. The dominant effect here is the steric interaction of the hydrocarbon to the surface, that is, the nonbonded or Pauli repulsion between the electrons in the CH_3 substituent with the surface. On the basis of $C(CH_3)_3$, the cost is ~7.8 kcal/mol per CH_3. The value for $CH_2(CH_3)$ is smaller by 1.6 kcal/mol, while the value per CH_3 for $CH(CH_3)_2$ is smaller by 2.0 kcal/mol. The smaller value

Table 6. Bond Lengths and Angles for CR_x/M_8 Clusters

A. M−C Bond Lengths (Å)

	CR_3 Series				CR_2 Series			CR Series	
metal	CH_3	CH_2CH_3	$CH(CH_3)_2$	$C(CH_3)_3$	CH_2	$CHCH_3$	$C(CH_3)_2$	CH	CCH_3
Pt	2.07	2.13	2.21	2.37	2.01	2.04	2.08	1.95	1.96
Ir	2.09	2.12	2.16	2.25	2.06	2.08	2.09	1.98	1.99
Os	2.12	2.14	2.18	2.24	2.08	2.10	2.15	2.02	2.03
Pd	2.01	2.05	2.08	2.14	1.98	2.00	2.07	1.93	1.94
Rh	2.04	2.08	2.08	2.12	2.01	2.03	2.05	1.95	1.97
Ru	2.10	2.12	2.16	2.24	2.03	2.05	2.10	1.98	2.00

B. Selected Bond Angles (deg)

		Pt	Ir	Os	Pd	Rh	Ru
CH_3	MCH	106	108	110	107	109	109
	HCH	112	111	109	112	109	109
CH_2Me	MCH	101	104	106	103	106	104
	MCC	116	117	117	115	116	118
$CHMe_2$	MCH	95	99	102	101	102	100
	MCC	113	114	115	110	113	115
CMe_3	MCC	108	111	111	109	111	111
	CC_MC	111	108	108	110	108	107
CH_2	MCM	88	83	83	88	85	84
	XCH[a]	125	125	127	125	126	126
CHMe	MCM	87	83	81	87	83	82
	XCH[a]	116	118	117	114	118	116
	XCC[a]	137	136	137	139	135	138
CMe_2	MCM	84	81	79	83	82	80
	CC_MC	104	106	104	105	106	104
CH	MCH	125	128	129	124	127	128
	MCM	91	87	85	91	87	86
CMe	MCC	125	128	129	126	128	130
	MCM	90	87	85	90	86	85

[a] X is the point on the metal surface such that C−*X* is perpendicular to the surface plane.

for the first and second methyl groups arises because steric repulsions can be decreased by increasing the C−C−M angle while compensating with a decrease in H−C−M angle. This compensation cannot occur in the trimethyl case.

These steric effects are also apparent in the M−C bond lengths. There is a significant increase in the M−C bond lengths for Pt from 2.08 → 2.13 → 2.21 → 2.37 Å for adding CH_3 groups. For the six metals, the average successive increase in M−C bond length is 0.035, 0.038, and 0.082 Å. For $C(CH_3)_3$ lengthening of the M−C bond is the only method to relieve steric repulsion.

3.1.2. CR_2 Series. For the series $CH_2 \rightarrow CHCH_3 \rightarrow C(CH_3)_2$, the average decrease in binding energy is 8.2 and 21.5 kcal/mol, respectively, compared to CH_2/M_8. The steric interactions for the fully methyl-substituted adsorbate is 10.8 kcal/mol per CH_3, substantially larger than for CR_3/M_8. This is because CR_2, adsorbs in a bridge site, putting the methyl groups closer to the surface. For example, CH_2/Pt_8 has a Pt−C bond length of 2.01 Å, leading to a surface to carbon distance of 1.45 Å (compared to 2.07 Å for CH_3). However, because the CR_2 total bond energy is twice as large, the decrease in bond energy for the fully substituted case is only 28% of the total bond energy for CR_2 but 48% for CR_3.

The steric effect for the singly substituted case, $CHCH_3$, is 2.6 kcal/mol smaller than the average for CR_2, since the methyl group can tilt away from the surface (the opposite H has little steric repulsion with the surface).

Substituting the first methyl increases M−C by 0.022 Å and the second methyl by 0.040 Å, much less than in the CR_3 series.

3.1.3. CR Series. There is an average 12.7 kcal/mol decrease in binding energy for the series $CH \rightarrow CCH_3$. This might seem strange since the methyl substituent is far from the surface, leading to very little steric interaction. In fact, this decrease arises from an electronic effect. In order for the CR adsorbate to form three bonds in the cap site, the CR fragment needs to have three unpaired spins. This corresponds to the $S = 3/2$ state of CR, but for both CH and CCH_3 the ground state is the $S = 1/2$ state. Thus, the process of bonding CR to the surface requires promoting the CR from the doublet to quartet state, reducing the bond energy by this amount. Indeed, the doublet to quartet excitation energies are calculated to be 19.7 and 32.4 kcal/mol for CH and CCH_3, respectively. This difference in excitation energy of 12.7 kcal/mol is expected to cause CCH_3 to have a bond energy 12.7 kcal/mol smaller than for CH, in exact agreement with the calculated number.

The average M−C bond lengths increase by only 0.013 Å between the two species, as expected from the similar bonding.

3.2. Charge-Transfer Effects. To estimate the effect of methyl substitution on charge transfer to the cluster, we calculated the Mulliken charges. Table 7 lists the Mulliken charges for four groups of atoms in CR_x/Pt_8: (1) R groups, (2) C atom in M−C bond, (3) M atoms involved in direct M−C bonding, and (4) M atoms not directly involved in M−C bonds.

The sum of these four groups is the overall charge of the cluster (zero since all the metal−adsorbate clusters are overall neutral). The other metals show qualitatively similar trends to Pt.

The total charge on the metal (sum of rows 3 and 4 of Table 7) becomes increasingly negative with increasing methyl substitution, indicating that C→M charge transfer occurs. This increased charge transfer from the hydrocarbon to the metal with increasing number of methyl groups is interpreted in terms of methyl inductive effects (electron donation), just as observed in organic compounds.

The charge on the C atom involved in the M−C bond (row 2) becomes increasingly positive with CH_3 substitution. We

Table 7. Mulliken Charges for CR_x/Pt_8

a. CR_3 Series

	CH_3	CH_2CH_3	$CH(CH_3)_2$	$C(CH_3)_3$
R group (organic ligands to C)	+0.56	+0.51	+0.47	+0.48
C atom in M−C bond	−0.25	−0.12	+0.01	+0.11
M atom in M−C bond	−0.42	−0.39	−0.34	−0.05
M atoms not in M−C bond	+0.11	+0.00	−0.14	−0.54

b. CR_2 Series

	CH_2	$CHCH_3$	$C(CH_3)_2$
R group (organic ligands to C)	+0.41	+0.38	+0.41
C atom in M−C bond	−0.34	−0.27	−0.08
M atoms in M−C bond	+0.08	+0.06	−0.01
M atoms not in M−C bond	−0.15	−0.17	−0.32

c. CR Series

	CH	CCH_3
R group (organic ligands to C)	+0.18	+0.18
C atom in M−C bond	−0.41	−0.34
M atoms in M−C bond	+0.12	+0.09
M atoms not in M−C bond	+0.11	+0.07

Table 8. Comparison of Adiabatic and Snap Bond Energies (in kcal/mol)

CR_x on Pt_8	adiabatic		snap	
CR_3/Pt_8				
CH_3	53.8	(+3.6)	57.4	
	(−5.2)			(−4.2)
CH_2CH_3	48.6	(+4.6)	53.2	
	(−6.5)			(−6.5)
$CH(CH_3)_2$	41.1	(+5.6)	46.7	
	(−10.1)			(−9.0)
$C(CH_3)_3$	31.0	(+6.7)	37.7	
CR_2/Pt_8				
CH_2	104.3	(+4.0)	108.3	
	(−6.2)			(−2.7)
$CHCH_3$	98.1	(+7.5)	105.6	
	(−13.3)			(−12.5)
$C(CH_3)_2$	84.8	(+8.3)	93.1	
CR/Pt_8				
CH	166.6	(+19.7)	186.3	
	(−11.9)			(+0.8)
CCH_3	154.7	(+31.4)	187.1	

[a] Numbers in parentheses indicate the difference between one row/column and the next row/column.

interpret this in terms of methyl group stabilization, just as observed in the stabilization of organic tertiary carbocations over secondary and primary.

Methyl substitution also tends to favor the planar form of CR_3 vs the pyramidal one. This leads to a significant increase in M−C bond lengths across the CR_3/M_8 species. Thus, CH_3/Pt_8 has a C−Pt bond of 2.07 Å while $C(CH_3)_3/Pt_8$ has a C−Pt bond length of 2.37 Å.

3.3. Snap Chemisorption Energies. The snap chemisorption energy is defined as the difference in energy between the adsorbate−metal cluster and the metal cluster infinitely separated from the adsorbate, but for which the structure of the adsorbate and metal cluster are frozen both at the geometry and spin state of the complex. That is, the adsorbate is not permitted to relax as the M−C bonds are broken. The snap bond energies of CR_x/Pt_8 are reported in Table 8 along with the corresponding adiabatic binding energies. The other metals show similar trends to Pt. The spin state of frozen CR_3 species is $S = 1/2$. CR_2 species are frozen at a spin state of $S = 1$, since two unpaired electrons are required to form two M−C bonds. CR species are frozen at a spin state of $S = 3/2$, since three unpaired electrons are required to form three M−C bonds. This includes the effect of the doublet-quartet excitation on the bond energy, discussed in section 3.1.3.

Whereas adiabatic binding energies are additive with the number of M−C bonds (Table 4), snap bond energies do *not* show this trend. The average M−C snap bond energies for CH_3, CH_2, and CH on Pt_8 are 57.4, 54.2, and 62.1 kcal/mol.

The difference between the snap bond energies of CH_3 and CH_2 can be attributed to strain energy in the Pt−C−Pt ring of the bridged CH_2/Pt_8 system. For CH_2/Pt_8 the Pt−C−Pt bond angle is 90°, while for CH_3/Pt_8 the Pt−C−H bond angles are 106°, closer to tetrahedral. This strain might well decrease the average bond energy by 3 kcal/mol for CH_2/Pt_8.

Increasing methyl substitution leads to decreasing snap bond energy for the CR_3 and CR_2 species, similar to the trend observed in adiabatic binding energies. There are some differences quantitatively; for example, the snap bond energy does not decrease as much as the adiabatic binding energy across the series. The lack of a direct steric effect on the snap bond energy for CR is plausible since the R group is far from the surface. However, CH in the cap position has an average M−C bond strength 4.7 kcal/mol higher than for CH_3. For the CR there is essentially no difference between the snap bond energy of CH and CCH_3, the full effect being accounted for by the doublet to quartet excitation energy (vide supra).

We believe that the increased bond strength of CR to cap sites is due to additional flexibility of the Pt orbitals to bind species to the cap site. In addition to the d orbitals localized on each Pt atom, the cap site can utilize the interstitial s-like orbital located in the triangle of the cap site (mixing with the d orbitals to create s−d hybrid orbitals). The added flexibility in the bond orbitals could be responsible for the increased Pt−C snap bond energy.

Experimental results confirm that methylidyne (CH) and ethylidyne (CCH_3) are the stable thermodynamic sinks at low temperature for C_1 and C_2 adsorbates on metals. This is most firmly established experimentally for ethylidyne on Pt(111).[35,36] Ethylidyne occupies a 3-fold fcc site and the C−C bond is perpendicular to the platinum surface. The experimental C−C and Pt−C bond lengths are 1.50 ± 0.05 and 2.00 ± 0.05 Å, respectively. Our calculations have the same geometry, with optimized C−C and Pt−C bond lengths of 1.49 and 1.96 Å, respectively. Studies on other closed packed surfaces relevant to our study include Ir(111),[37] Pd(111),[38] Rh(111),[39] and Ru(0001).[40]

4. Thermochemical Computations

We will now consider how to use the bond energies from QM calculations to estimate the bond energies and heats of formation of more complex chemisorbed species. Experimental heats of formation and bond energies quoted here were obtained from ref 41.

4.1. Group Additivity Values. On the basis of heats of formation calculated from QM for the $CH_m(CH_3)_n$ species, we

(35) Kesmodel, L. L.; Dubois, L. H.; Somorjai, G. A. *J. Chem. Phys.* **1979**, *70*, 2180.
(36) Starke, U.; Barbieri, A.; Materer, N.; Van Hove, M. A.; Somorjai, G. A. *J. Phys. Chem.* **1993**, *286*, 1.
(37) Marinova, Ts. S.; Chakarov, D. V. *Surf. Sci.* **1987**, *192*, 275.
(38) Gates, J. A.; Kesmodel, L. L. *Surf. Sci.* **1983**, *124*, 68.
(39) Dubois, L. H.; Castner, D. G.; Somorjai, G. A. *J. Chem. Phys.* **1980**, *72*, 5234.
(40) Barteau, M. A.; Broughton, J. Q.; Menzel, D. *Appl. Surf. Sci.* **1984**, *19*, 92.
(41) Lide, D. R. *Handbook of Chemistry and Physics*, 74th ed.; CRC Press: Boca Raton, FL, 1993−1994.

Table 9. Group Values (kcal/mol) for Various Species

a. $C-M_k(C)_n(H)_{4-k-n}$ (see Section 4.1)

	Pt	Ir	Os	Pd	Rh	Ru
$C-M(H)_3$	−14.82	−11.91	−7.81	−11.06	−10.62	−1.40
$C-M(C)(H)_2$	−6.32	−3.73	+2.85	−1.04	−1.44	+8.96
$C-M(C)_2(H)$	+4.02	+6.76	+11.32	+11.26	+7.77	+19.86
$C-M(C)_3$	+17.18	+22.06	+22.41	+22.88	+19.44	+34.36
$C-M_2(H)_2$	−4.05	−1.11	+4.09	+0.45	+2.25	+10.05
$C-M_2(C)(H)$	+2.88	+8.87	+12.95	+7.61	+11.18	+17.86
$C-M_2(C)_2$	+14.73	+21.59	+28.39	+21.45	+18.98	+31.43
$C-M_3(H)$	−16.12	−10.94	−5.28	−3.66	−5.92	+5.55
$C-M_3(C)$	−16.83	−12.18	−4.09	−4.90	−4.81	+6.96

b. $C-M(C_M)(C)_{n-1}(H)_{3-n}$ (see Section 4.3)

	Pt	Ir	Os	Pd	Rh	Ru
$C-M(C_M)(H)_2$	−10.57	−7.82	−2.48	−6.05	−6.03	+3.78
$C-M(C_M)(C)(H)$	−1.15	+1.52	+7.09	+5.11	+3.17	+14.41
$C-M(C_M)(C)_2$	+10.60	+14.41	+16.87	+17.07	+13.61	+27.11

c. $C-(C)_n(H)_{4-n}$ from ref 6 (see Sections 4.1, 4.3, 4.4)

$C-(C)(H)_3$	−10.20
$C-(C)_2(H)_2$	−4.93
$C-(C)_3(H)$	−1.90

can assign group values in a scheme analogous to Benson group additivities. The heats of formation are calculated using three reference compounds: the M_8 metal cluster ($\Delta H_f = 0$), gas-phase CH_4 ($\Delta H_f = -17.9$ kcal/mol), and gas-phase C_2H_6 ($\Delta H_f = -20.0$ kcal/mol).

This yields atomic H_f values required to convert from QM data (in hartree) to thermochemical data referenced to standard states [E(C) = −38.12718 and E(H) = −0.59209 hartree]. This provides implicit first-order corrections for zero point energy and enthalpy changes at room temperature (discussed in section 2.1). CH_4 and C_2H_6 were chosen, rather than CH_4 and H_2, because they are expected to provide a better implicit correction in the case of adsorbates containing C−C bonds. We would expect that the QM results would have systematic errors proportional to the number of bonds; however, we make no such empirical corrections here. The resulting group values are shown in Table 9a.

An example of how these are assigned is as follows. The calculated heat of formation of CH_3 on Pt_8 can be written in terms of two group contributions:

$$-14.82 \text{ kcal/mol} = [C-(Pt)(H)_3] + [Pt-(C)]$$

We will take

$$[Pt-(C)] = 0$$

so that

$$[C-(Pt)(H)_3] = -14.82 \text{ kcal/mol}$$

The calculated heat of formation of CH_2CH_3 on Pt_8 is written as

$$-16.52 \text{ kcal/mol} = [C-(Pt)(C)(H)_2] + [C-(C)(H)_3]$$

Since $[C-(C)(H)_3] = -10.20$ (used by Benson[8]), we obtain

$$[C-(Pt)(C)(H)_2] = -6.32 \text{ kcal/mol}$$

Table 9 allows one to predict the relative stability of surface hydrocarbons. For example, considering the isopropyl and *n*-propyl isomers, the heats of formation predicted from group additivities are

$$H_f(i\text{-}C_3H_7/Pt) = [C-(Pt)(C)_2(H)] + 2[C-(C)(H)_3] = +4.02 + 2(-10.20) = -16.38 \text{ kcal/mol}$$

$$H_f(n\text{-}C_3H_7/Pt) = [C-(Pt)(C)(H)_2] + [C-(C)_2(H)_2] + [C-(C)(H)_3] = -6.32 - 4.93 - 10.20 = -21.45 \text{ kcal/mol}$$

Here we use the Benson group values for cases that do not involve the metal. Thus we predict that *n*-C_3H_7 chemisorbs more strongly to Pt than *i*-C_3H_7 by 5.1 kcal/mol. Indeed, we carried out QM calculations for these two species (on Pt_8) and find an energy difference of 6.4 kcal/mol (within 1.3 kcal/mol of the group additivity value). These results are summarized in Table 10, along with predictions of the relative energies for various butyl radicals chemisorbed on Pt to further illustrate the process.

Table 10. Group Additivity Predictions (kcal/mol) for Propyl and Butyl Adsorbed on Pt

	grp add prediction		QM calculation	
	ΔH_f	substituent effect	ΔH_f	substituent effect
i-Pr/Pt	−16.38	5.1	−16.38	6.4
n-Pr/Pt	−21.45	0.0	−22.82	0.0
t-Bu/Pt	−13.42	13.0		
i-Bu/Pt	−21.31	5.1		
n-Bu/Pt	−26.38	0.0		

4.2. Bond Additivities of Di-σ Adsorbed Species. In this section, we use only calculated values with no zero point or room-temperature enthalpy corrections. This provides a comparison to the next section on group additivities (Section 4.3) where implicit first order corrections have been included into the heats of formation.

4.2.1. The di-σ Bond of Ethylene to the Surface. The process of converting ethane to ethylene can be written as

$$H_3C-CH_3 \xrightarrow{D(C-H)} H + H_2C-CH_3 \xrightarrow{D(C-H)-\pi} 2H + H_2C{=}CH_2 \xrightarrow{-D(H-H)} H_2 + H_2C{=}CH_2 \quad (1)$$

Thus the heat of reaction is

$$\Delta H_{rxn} = 2D(C-H) - \pi - D(H-H) \quad (2)$$

where π is the energy of the CC π bond. From QM we calculate $\Delta H_{rxn} = +41.7$ kcal/mol. Using the QM values of $D(C-H) = 109.7$, and $D(H-H) = 111.7$ leads to

$$\pi^{qm} = 2D(C-H) - D(H-H) - \Delta H_{rxn} = 219.4 - 111.7 - 41.7 = 66.0 \text{ kcal/mol}$$

as the QM value π bond strength for C_2H_4.

Using instead the experimental numbers of $\Delta H_f(C_2H_6) = -20.02$, $\Delta H_f(C_2H_4) = +12.55$, $D(C-H) = 100.5$, and $D(H-$

(42) This value differs slightly from the one (−13.06) implicit in Figure 3, because the reference compounds are now CH_4 and C_2H_6. Using the derived value of $E(H) = 0.59209$ yields $H_f[H_{ads}] = -9.62$ kcal/mol. Hence, $H_f[(CH_3)_{ads} + (H)_{ads}] = -14.82 - 9.62 = -24.44$ kcal/mol. Section 2 (and Figure 3) use CH_4 and H_2 as reference compounds, and hence the heat of formation of adsorbed CH_3 is −13.06 kcal/mol. However, now $H_f[H_{ads}] = -11.38$ kcal/mol. Hence, $H_f[(CH_3)_{ads} + (H)_{ads}] = -13.06 - 11.38 = -24.44$ kcal/mol, the same value as using CH_4 and C_2H_6 as reference compounds.

Table 11. Results from QM Calculations of Ethylene, *cis*-Butene, and 2,3-Dimethylbut-2-ene on Pt_8

adsorbate	total energy (hartree)	BE[a] (kcal/mol)	selected bond distances (Å)	π^{QM} (kcal/mol)[b]	D(M−C)[b]	D(M−M)[c]
C_2H_4	−1031.90852	36.1	Pt−C 2.06, C−C 1.52	66.0	51.2	+0.3
cis-C_4H_8	−1110.53844	30.1	Pt−C 2.10, C−C 1.53	57.4	44.9	+2.3
$C_2(CH_3)_4$	−1189.15174	16.4	Pt−C 2.14, C−C 1.58	50.0	36.1	+5.8

[a] Calculated from E(*cis*-butene) = −157.23323 hartree and E(2,3-dimethylbut-2-ene) = −235.86839 hartree. [b] Calculated from Table 5 using averages as discussed in section 4.2. [c] Calculated as described in section 4.2 using QM results.

Table 12. QM and Bond Additivity Calculations of C_2H_4/M_8

M	total energy (hartree)	selected distances (Å)	QM BE[a] (kcal/mol)	D(M−C)[b] (kcal/mol)	bond add. BE[c] (kcal/mol)	D(M−M)[d] (kcal/mol)
Pt	−1031.90852	Pt−C 2.06; C−C 1.52	36.1	51.2	36.4	+0.3
Ir	−916.05391	Ir−C 2.08; C−C 1.53	34.0	48.5	31.0	−3.0
Os	−806.63625	Os−C 2.14; C−C 1.52	20.7	43.1	20.2	−0.5
Pd	−1092.63192	Pd−C 2.07; C−C 1.46	32.9	46.7	27.4	−5.5
Rh	−954.62570	Rh−C 2.05; C−C 1.51	28.0	46.7	27.4	−0.6
Ru	−829.44775	Ru−C 2.11; C−C 1.50	12.2	36.9	7.8	−4.4

[a] Calculated from QM using $E(C_2H_4)$ = −78.59380 hartree and E(M) from last column of Table 1. [b] Calculated using [D(M−CH_3) + D(M−C_2H_5)]/2 from Table 5. [c] Calculated as described in section 4.2.1 using π^{qm} = 66.0 kcal/mol. [d] Average value for D(M−M) is −2.3 kcal/mol.

H) = 104.20 would lead to the thermochemical value of

$$\pi^{tc} = 2D(C{-}H) - D(H{-}H) - \Delta H_{rxn} = 201.0 - 104.2 - 32.5 = 64.3 \text{ kcal/mol}$$

Both numbers are quite close to the experimental rotational barrier in ethylene of π^{exp} = 65 kcal/mol.[43]

Consider now the di-σ bond of ethylene to the metal surface. We can *predict* this number in an analogous fashion as

$$M{-}CH_2{-}CH_2{-}M \xrightarrow[D(M-C)]{} M + CH_2CH_2{-}M \xrightarrow[D(MC)-\pi]{} 2M + H_2C{=}CH_2 \xrightarrow[-D(M-M)]{} M_2 + H_2C{=}CH_2$$

This time we write

$$\Delta H_{rxn} = 2D(M{-}C) - \pi - D(M{-}M) \quad (3)$$

The question now is which value to use for D(M−C) for the M−CH_2CH_2−M system. We have two choices. Electronically D(M−CH_2CH_3) is more similar to the D(M−CH_2CH_2M) system since C in the M−C bond also has an additional C−C bond. Sterically D(M−CH_3) is more similar to D(M−CH_2CH_2M) since after forming the second bond to the surface, neither C causes steric repulsion with the surface. The most rigorous approach would be to carry out a series of calculations to separate the steric and electronic contributions due to methyl substitution.

A simple alternative which we use here is to use the average value. Hence for C_2H_4/Pt_8, we use

$$D(M{-}C) = [D(Pt{-}CH_3) + D(Pt{-}CH_2{-}CH_3)]/2 = (53.8 + 48.6)/2 = 51.2 \text{ kcal/mol}$$

Using this value for D(M−C),

$$BE(H_2C{=}CH_2/Pt_8) = 2 \times 51.2 - 66.0 - D(M{-}M) = 36.4 - D(M{-}M)$$

The calculated QM binding energy is 36.1 kcal/mol. Thus we obtain D(M−M) = +0.3 kcal/mol (see Table 11). Coverage-dependent microcalorimetry measures an adsorption energy ranging from 30 to 48 kcal/mol.[23] The C−C bond is parallel to and found above a Pt−Pt bridge. The molecular plane of C_2H_4 is tilted and the C−C bond length measured from NEXAFS is 1.49 ± 0.04 Å.[44] This compares to our calculated C−C bond length of 1.51 Å.

For all six metals, Table 12 compares the di-σ bond of ethylene predicted using these bond additivity concepts (assuming π^{qm} = 66.0 kcal/mol) with the QM value (we report the value of D(M−M) required to make the two consistent). The average value is D(M−M) = −2.3 kcal/mol. Thus we take the average strain for the M_2C_2 cyclobutane to be −2.3 kcal/mol. Using this average value we would have predicted the di-σ bond energies for all six metals to within ∼3 kcal/mol of the QM result.

4.2.2 The Di-σ Bond of *cis*-Butene to Pt Surface. As a second example, consider the bond energy of *cis*-2-butene to Pt surface. The process of converting *n*-butane to *cis*-2-butene can be written as

$$n\text{-}C_4H_{10} \xrightarrow[D(C-H)]{} H + CH(CH_3)(C_2H_5) \xrightarrow[D(C-H)-\pi]{} 2H + cis\text{-}C_4H_8 \xrightarrow[-D(H-H)]{} H_2 + cis\text{-}C_4H_8$$

Using the QM values of ΔH_{rxn} = +32.1, D(C−H) = 100.6, and D(H−H) = 111.7 leads to

$$\pi^{qm} = 2D(C{-}H) - D(H{-}H) + \Delta H_{rxn} = 2 \times 100.6 - 111.7 - 32.1 = 57.4 \text{ kcal/mol}$$

which is 8.6 kcal/mol weaker than in ethylene.

Consider now the bonding of *cis*-butene to the metal surface. Following the reasoning in section 4.2.1 we consider that

$$BE[cis\text{-}(CH_3)HC{=}CH(CH_3)/M_8] = 2D(M{-}C) - \pi - D(M{-}M)$$

Since D(Pt−C_2H_5) = 48.6 and D(Pt−C_3H_7) = 41.1, we assign D(M−C) = 44.9 kcal/mol (average of the two) and obtain

$$BE[cis\text{-}(CH_3)HC{=}CH(CH_3)/M_8] = 2 \times 44.9 - 57.4 - D(M{-}M) = 32.4 - D(M{-}M)$$

The calculated QM binding energy is 30.1 kcal/mol (Table 11). Thus we obtain D(M−M) = +2.3 kcal/mol, which is 2.0 kcal/mol higher than for C_2H_4. Thus, bond additivity predicts a small increase in strain in the cyclic M_2C_2 unit.

(43) Merer, A. J.; Mulliken, R. S. *Chem. Rev.* **1969**, *69*, 639.

(44) Stohr, J.; Setter, F.; Johnson, A. L. *Phys. Rev. Lett.* **1984**, *53*, 1684.

Table 13. Predicted Adiabatic Binding Energies (kcal/mol) from Bond Additivity of *cis*-Butene and 2,3-Dimethylbut-2-ene

	cis-butene			2,3-dimethylbut-2-ene		
	D(M−M)[a]	D(M−C)[b]	BE[c]	D(M−M)[d]	D(M−C)[e]	BE[f]
Pt	+2.3	44.9	30.1	+5.8	36.1	16.4
Ir	−1.0	42.2	28.0	+2.5	32.3	12.1
Os	+1.5	36.6	14.3	+5.0	29.8	4.6
Pd	−3.5	38.6	23.3	+0.0	29.6	9.2
Rh	+1.4	40.6	22.4	+4.9	33.1	11.3
Ru	−2.4	29.3	3.6	+1.1	19.6	−9.7

[a] Predicted from QM results for Pt by adding 2.0 kcal/mol to D(M−M) in Table 12. [b] Calculated using [D(M−C_2H_5) + D(M−C_3H_7)]/2 in Table 5. [c] Calculated using predicted D(M−M), π^{qm} = 57.4 in Table 12, and corrected D(M−C). [d] Predicted from QM results for Pt by adding 5.5 kcal/mol to D(M−M) in Table 12. [e] Calculated using [D(M−C_3H_7) + D(M−C_4H_9)]/2 in Table 5. [f] Calculated using predicted D(M−M), π^{qm} = 50.0 in Table 12, and corrected D(M−C).

Assuming this increase of strain by 2.0 kcal/mol, we can estimate the D(M−M) for the other five metals. This leads then to predictions of the di-σ bond energies for bonding *cis*-2-butene to the other metals using

$$\mathrm{BE}[\textit{cis}\text{-}(CH_3)HC{=}CH(CH_3)/M_8] = 2D(\mathrm{M{-}C}) - \pi^{qm} - D(\mathrm{M{-}M})$$

where D(M−C) is calculated from the average of M−C_2H_5 and M−C_3H_7 binding energies. These results are summarized in Table 13. Noteworthy here is that *cis*-butene is predicted to bind quite weakly to Ru.

4.2.3. The Di-σ Bond of 2,3-Dimethylbut-2-ene (tetramethylethylene) to Pt Surface. As a third example, consider the bond energy of 2,3-dimethylbut-2-ene [$(CH_3)_2C{=}C(CH_3)_2$] to the Pt surface. The process of converting 2,3-dimethylbutane [$(CH_3)_2HC{-}CH(CH_3)_2$] to $(CH_3)_2C{=}C(CH_3)_2$ can be written as

$$[(CH_3)_2HC{-}CH(CH_3)_2] \xrightarrow[D(\mathrm{C-H})]{} H + [(CH_3)_2C{-}CH(CH_3)_2] \xrightarrow[D(\mathrm{C-H})-\pi]{}$$
$$2H + (CH_3)_2C{=}C(CH_3)_2 \xrightarrow[D(\mathrm{H-H})]{} H_2 + (CH_3)_2C{=}C(CH_3)_2$$

Using the QM values of ΔH_{rxn} = +27.5, D(C−H) = 94.6, and D(H−H) = 111.7 leads to

$$\pi^{qm} = 2D(\mathrm{C{-}H}) - D(\mathrm{H{-}H}) + \Delta H_{rxn} = 2 \times 94.6 - 111.7 - 27.5 = 50.0 \text{ kcal/mol}$$

which is 7.4 kcal/mol weaker than in *cis*-butene and 16.0 kcal/mol weaker than in ethylene.

Consider now the bonding of $(CH_3)_2C{=}C(CH_3)_2$ to the metal surface, we write

$$\mathrm{BE}[(CH_3)_2C{=}C(CH_3)_2/M_8] = 2D(\mathrm{M{-}C}) - \pi - D(\mathrm{M{-}M})$$

Since D(Pt−C_3H_7) = 41.1 and D(Pt−C_4H_9) = 31.0, we assign D(M−C) = 36.1 kcal/mol, leading to

$$\mathrm{BE}[(CH_3)_2C{=}C(CH_3)_2/M_8] = 2 \times 36.1 - 50.0 - D(\mathrm{M{-}M}) = 22.2 - D(\mathrm{M{-}M})$$

The calculated QM binding energy is 16.4 kcal/mol (Table 11). Hence, D(M−M) = +5.8 kcal/mol, which is 3.5 kcal/mol larger than for *cis*-butene and 5.5 kcal/mol larger than for ethylene.

Assuming this increase of strain by 5.5 kcal/mol from ethylene, we can estimate the D(M−M) for the other five metals as outlined in section 4.2.2. Again D(M−C) is calculated as the average of M−C_3H_7 and M−C_4H_9 binding. Using the same equation

$$\mathrm{BE}[(CH_3)_2C{=}C(CH_3)_2/M_8] = 2D(\mathrm{M{-}C}) - \pi^{qm} - D(\mathrm{M{-}M})$$

we can predict the binding energy of $(CH_3)_2C{=}C(CH_3)_2$ to the other five metals. The results, summarized in Table 13, predict that $(CH_3)_2C{=}C(CH_3)_2$ binds weakly to Os and does not bind to Ru.

Comparing the strain of di-σ bonds for ethylene, *cis*-2-butene, and 2,3-dimethylbut-2-ene, we find the strain associated with the M_2C_2 unit increases slightly from +0.3 to +2.3 to +5.8 kcal/mol.

4.3. Modified Group Additivities To Predict Di-σ Chemisorbed Species on Metals. The discussions in sections 4.1 and 4.2 suggest that for bonding olefins to metal surfaces the group function [C−MC_nH_{3-n}] be modified to the form [C−MC_M-$C_{n-1}H_{3-n}$] to reflect the decreased steric effects for adding the second bond to the surface. Effectively we can calculate these values as

$$[\mathrm{C{-}MC_MC_{n-1}H_{3-n}}] = \{[\mathrm{C{-}MC_nH_{3-n}}] + [\mathrm{C{-}MC_{n+1}H_{2-n}}]\}/2$$

where the [C−MC_nH_{3-n}] and [C−$MC_{n+1}H_{2-n}$] values are from Table 9a. Thus (for M = Pt),

$$[\mathrm{C{-}M(C_M)(H)_2}] = (-14.82-6.32)/2 = -10.57 \text{ kcal/mol}$$

$$[\mathrm{C{-}M(C_M)(C)(H)}] = (-6.32 + 4.02)/2 = -1.15 \text{ kcal/mol}$$

$$[\mathrm{C{-}M(C_M)(C)_2}] = (4.02 + 17.18)/2 = +10.60 \text{ kcal/mol}$$

These terms are tabulated in Table 9b.

Using these group additivities we can predict the heat of formation of ethylene bonded to Pt (di-σ) to form a M_2C_2 four-membered ring on the metal surface.

$$H_f(C_2H_4/Pt) = 2[\mathrm{C{-}M(C_M)(H)_2}] = 2(-10.57) = -21.14 \text{ kcal/mol}$$

which compares to the QM value of −17.9 kcal/mol. We interpret this reduction by 3.2 kcal/mol in the bonding to the surface as *strain energy* due to the M_2C_2 four-membered ring unit.

Similarly, the heat of formation of chemisorbed *cis*-(CH_3)-HC=$CH(CH_3)$ is predicted to be

$$H_f[\textit{cis}\text{-}(CH_3)HC{=}CH(CH_3)/Pt] = 2[\mathrm{C{-}M(C_M)(C)(H)_2}] - 2[\mathrm{C{-}C(H)_3}]$$
$$= 2(-1.15) - 2(-10.20) = -22.70 \text{ kcal/mol}$$

which compares to the QM value of −22.4 kcal/mol. Thus the strain energy due to the M_2C_2 unit is 0.3 kcal/mol.

For $(CH_3)_2C{=}C(CH_3)_2$/Pt, we predict the heat of formation of chemisorbed $(CH_3)_2C{=}C(CH_3)_2/M_8$ to be

$$H_f[(CH_3)_2C{=}C(CH_3)_2/Pt] = 2[\mathrm{C{-}M(C_M)(C)_2(H)}] - 4[\mathrm{C{-}C(H)_3}]$$
$$= 2(10.60) - 4(-10.20) = -19.60 \text{ kcal/mol}$$

which compares to the QM value of −16.5 kcal/mol. Thus we assign the strain energy due to the M_2C_2 unit as 3.1 kcal/mol.

Table 14. Predicted H_f, Calculated H_f, and Strain Energy of Ethylene, *cis*-Butene, and 2,3-Dimethylbut-2-ene on Pt_8 (in kcal/mol)

adsorbate	group add H_f (predicted)[a]	QM H_f (calculated)	strain energy[b,c]
C_2H_4	−21.1	−17.9	+3.2
cis-C_4H_8	−22.7	−22.4	+0.3
$C_2(CH_3)_4$	−19.6	−16.5	+3.1

[a] Calculated from Tables 9b−c. [b] Strain energy = $H_f^{QM} - H_f^{GA}$. [c] Average strain energy = +2.2 kcal/mol.

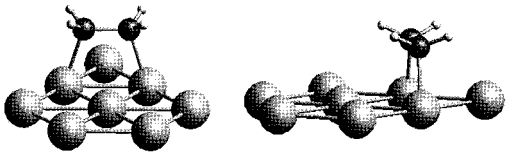

Figure 5. C_2H_4 adsorbed on M_8.

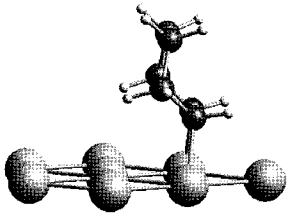

Figure 6. C_6H_{10} adsorbed on Pt_8.

These results suggest that that there is little increase in strain energy in the M_2C_2 unit due to substitution of methyl groups. The average strain energy is 2.2 kcal/mol. The results are summarized in Table 14. This differs from the D(M−M) values calculated in section 4.2, where the apparent strain increases with substitution. The difference in these two approaches is that the group values in this section include implicitly zero point energy and enthalpy corrections to room temperature. Since larger adsorbates have a larger zero point energy correction, the binding energy is reduced. In this view the more flexible metal−carbon bonds can adjust to keep the strain energy low. This contrasts with cyclobutane C_4 units, where stiff C−C bonds lead to a large strain energy and a Benson ring strain correction of 26 kcal/mol.

Assuming similar strain energies as Pt (or an average of 2.2 kcal/mol) in the other five metals leads to predictions of the heat of formation for *cis*-butene and $(CH_3)_2C{=}C(CH_3)_2$, in a way analogous to predicting binding energies discussed in sections 4.2.2 and 4.2.3.

4.4. Use of Group Additivities to Predict Chemisorbed Cyclohexene on Pt. To investigate the applicability of strain energy concepts, consider chemisorption of cyclohexene (c-C_6H_{10}) in a 1,2-di-σ conformation to the Pt surface (see Figure 6). The heat of formation of C_6H_{10}/Pt predicted using group additivity is

$$H_f(c\text{-}C_6H_{10}/Pt) = 2[C-M(C_M)(C)(H)_2] + 4[C-(C)_2(H)_2]$$
$$= 2(-1.15) + 4(-4.93) +$$
$$\text{strain energy} = -22.02 + \text{strain energy}$$

The strain energy has two components. (1) The structure of the M_2C_2 unit of C_6H_{10}/Pt_8 is similar to ethylene and its methyl-substituted derivatives. Hence, we can apply an average strain energy component of 2.2 kcal/mol calculated for C_2H_4/Pt_8 to this system. (2) On a flat surface the C_6 ring cannot have its favored chair form; instead it is promoted to the boat conformation (only slightly distorted from boat cyclohexane; see Figure 6). The boat to chair transition is ∼6.0 kcal/mol, giving an additional 6.0 kcal/mol of ring strain.

Thus, we expect

$$H_f(C_6H_{10}/Pt) = -22.0 + 6.0 + 2.2 = -13.8 \text{ kcal/mol}$$

The calculated QM value is −12.6 kcal/mol, only 1.2 kcal/mol different. Thus using group additivity, one can predict the chemisorption of chemisorbed intermediates within a few kilocalories/mole.

4.5 How To Use These Values: A Recipe. The following steps summarize how to apply the derived group values to calculate the heat of formation for a hydrocarbon bound to a metal surface:

(1) Apply group values in Table 9 for carbons directly bound to the metal surface.

(2) Apply Benson group values for carbons *not* bound to the metal surface (some selected values are in Table 9c).

(3) Assume that the strain energy for an M_2C_2 unit is 2.2 kcal/mol (the average value from Table 14).

(4) Apply Benson strain energies for strain in any fully hydrocarbon ring. Also additional strain energies due to nonideal conformations (e.g. chair to boat) should be added here.

(5) Add the numbers from steps (1−4).

Relative comparison among purely organic molecules using Benson group values are good to within 1 kcal/mol. Our predictions of relative energies of adsorbed species have a slightly larger spread, in the range of 1.5 kcal/mol.

5. Conclusions

We find that the C bonded to the closest packed surface of Pt, Ir, Os, Pd, Rh, and Ru, always prefers the site in which this C has four σ bonds. The adiabatic binding energies are roughly additive according to the number of M−C σ bonds formed and decrease with increasing methyl substitution for all CR_x. These effects due to substitution are similar for the various metals.

The computed energetics are used to obtain a group additivity scheme for predicting binding energies of hydrocarbons chemisorbed to metal surfaces. We provide several examples to illustrate how nine new group values for M−C bonding can be combined with existing Benson group additivities to make useful predictions. This allows two types of estimates: (i) predicting binding energies and heats of formation of larger and more complex hydrocarbons on the same metal and (ii) predicting how changing the metal will change the energetics for the same organic fragments.

This provides a new powerful technique for deriving a mechanistic understanding of complex hydrocarbon reactions and rearrangements on catalytic surfaces.

6. Computational Approach

6.1. The M_8 Cluster Model. On the basis of a series of computations for the electronic structures of Pt_N clusters, we developed the interstitial electron model (IEM) for bonding that explained the details of the ground electronic states in terms of a simple orbital model.[10] The IEM suggests that the surface atoms of the (111) surface of crystalline Pt have valence electrons in a $6s^15d^9$ electronic configuration. This suggests that to mimic the chemistry for Pt(111) surfaces, a cluster model should lead to a ground state with the s^1d^9 electronic configu-

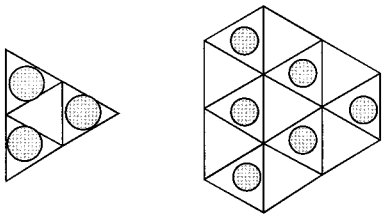

Figure 7. Pt_6 and Pt_{12} planar clusters.

Table 15. Bulk M−M Distances Used in Cluster Calculations (ref 56)

metal	M−M distance (Å)	metal	M−M distance (Å)
Pt	2.775	Pd	2.750
Ir	2.714	Rh	2.689
Os	2.734	Ru	2.706

ration at each atom. In addition, it should provide internal binding sites containing the on-top, 2-fold bridge, and 3-fold cap sites characteristic of closest packed surfaces [(111) for fcc and (0001) for hcp].

We found the Pt_8 planar cluster (Figure 1) to be the simplest choice satisfying these two properties. Altogether there are 80 valence electrons in Pt_8. This eight-atom cluster has four interstitial orbitals and hence eight of the 80 electrons are located in these predominantly s bonding orbitals. The remaining 72 electrons are in d orbitals. Hence, the configuration is s^8d^{72} or s^1d^9 per Pt. A simple rule is that clusters with a 2:1 ratio of number of atoms to interstitial orbitals will have the desired s^1d^9 configuration. The planar Pt_6 triangle (Figure 7) with three interstitial orbitals also has an s^1d^9 configuration but does not have an internal on-top binding site. The planar Pt_{12} cluster (Figure 7) with six interstitial orbitals, on the other hand, completely encloses the on-top, bridge, and 3-fold (cap) binding sites. It also has the desired s^1d^9 configuration. The calculated binding energies of CH_3, CH_2, and CH to this Pt_{12} cluster are similar to the Pt_8 cluster, suggesting that the latter is indeed the most economical choice.

From similar studies on the five metals (Ir, Os, Pd, Rh, and Ru), we also find that the M_8 cluster generally has the desired s^1d^{N-1} configuration. Since Pt, Ir, Pd, and Rh are fcc metals, this cluster models the (111) surface. For Os and Ru, which have hcp packing, the M_8 cluster models the (0001) surface.

Our calculations take the M−M bonds in each cluster to be the bond distance in the bulk crystal (see Table 15). This is because we consider that particles in the real catalyst are sufficiently large to enforce this structure. Slab calculations suggest that binding energies increase by 2−3 kcal/mol when the top layer of a slab is allowed to relax.[45]

For the optimal (most stable) binding sites, the chemisorbed organics were fully optimized on the cluster. For CH_x in nonoptimal sites, we generally had to apply a constraint to keep the fragment in the nonoptimal site. All methyl-substituted adsorbates were allowed to freely optimize, but they were studied only in the optimal binding sites.

The M_8 cluster only models conditions close to the zero coverage limit. It is expected that at higher coverages, binding energies (and corresponding derived group values) may change. Modeling large complicated adsorbates that have steric interactions with a larger surface area of the metal would require a larger metal cluster. The group values derived in this paper may change systematically by a few kilocalories/mole for a different metal cluster with an s^1d^{N-1} configuration.

(45) Ge, Q.; King, D. A. *J. Chem. Phys.* **1999**, *110*, 4699.

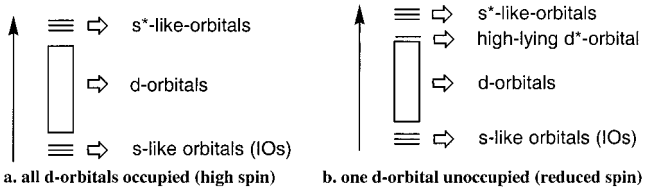

Figure 8. Schematic energy diagram for metal clusters.

6.2. Details for QM Computations. Calculations were carried out using the restricted B3LYP flavor of density functional theory (DFT), which includes nonlocal corrections (generalized gradient approximation) and exact Hartree−Fock (HF) exchange operators with the Slater local exchange functional.[46] We use the parameters referred to as Becke3[47] with the Becke nonlocal gradient correction,[48] the Vosko−Wilk−Nusair exchange functional,[49] and the Lee−Yang−Parr local and nonlocal correlation functional.[50]

All calculations were carried out using the Jaguar program.[51,52] The metals were described using the Hay and Wadt core-valence relativistic effective-core potential (ECP) with 18 explicit electrons for Pt, Pd; 17 electrons for Ir, Rh; and 16 electrons for Os, Ru (denoted LACVP in Jaguar).[53] This is a nonlocal ECP using angular momentum projection operators to enforce the Pauli principle.[54,55] All electrons were considered for carbon and hydrogen using the 6-31G** basis set.

6.3 Spin States. The various spin states were calculated as pure spin states (not unrestricted DFT). The optimum spin of the metal−adsorbate complex is determined by separate calculations of all low-lying spins where in each case the geometric structure for each adsorbate on the metal surface was fully optimized (but M−M bonds kept fixed).

To ensure that we have the correct spin and occupation for each system, we went through an extensive procedure to determine the optimum orbital configuration for each spin and to consider all possible low lying spins. For example, consider Pt_8. We find that the ground-state spin is $S = 3$. In addition to low-lying excited states of $S = 3$, the lowest energy $S = 4$ state is higher by 1.4 kcal/mol. We consider each of these configurations in bonding various intermediates to the surface.

The IEM predicts that for small clusters, the low-lying s bonding orbitals are always doubly occupied, the high-lying s antibonding orbitals are always empty, and the d orbitals are filled in the high-spin configuration. This is illustrated by the schematic in Figure 8a. As the clusters get larger, it becomes more favorable to spin-pair electrons in the high-lying d orbitals (Figure 8b). This is what happens in Pt_8, where the high-spin $S = 4$ is less favorable than the lower spin $S = 3$ state. Further examples of this can be found in ref 10.

Upon binding say CH_2 to the surface, we expect that the two unpaired electrons of triplet CH_2 will be paired with two electrons from the metal to form an $S = 2$ ground state for the CH_2/Pt_8 cluster. However, we calculated the energies of the S

(46) Slater, J. C. *Quantum Theory of Molecules and Solids*, Vol. 4: *The Self-Consistent Field for Molecules and Solids*, Mc-Graw Hill: New York, 1974.
(47) Becke, A. D. *J. Chem. Phys.* **1993**, *98*, 5648.
(48) Becke, A. D. *Phys. Rev. A* **1988**, *38*, 3098.
(49) Vosko, S. H.; Wilk, L.; Nusair, M. *Can. J. Phys.* **1980**, *58*, 1200.
(50) Lee, C.; Yang, W.; Parr, R. G. *Phys. Rev. B* **1988**, *37*, 785.
(51) Jaguar 3.5, Schrodinger, Inc., Portland, Oregon, 1998.
(52) Greeley, B. H.; Russo, T. V.; Mainz, D. T.; Friesner, R. A.; Langlois, J.-M.; Goddard, III, W. A., Honig, B. *J. Am. Chem. Soc.* **1994**, *116*, 11875.
(53) Hay, P. J.; Wadt, W. R. *J. Phys. Chem.* **1985**, *82*, 299.
(54) Goddard, W. A., III *Phys. Rev.* **1968**, *174*, 659.
(55) Melius, C. F.; Olafson, B. O.; Goddard, W. A., III *Chem. Phys. Lett.* **1974**, *28*, 457.
(56) Winter, M. http://www.shef.ac.uk/chemistry/web-elements/.

$= 1$, $S = 2$, and $S = 3$ states. The result from the calculations is that $S = 2$ is indeed the ground state. It is also necessary to check all low-lying orbital configurations for a given spin to ensure that the ground-state energy is found. Depending on the initial guess, the wave function may converge to a state that is 2−3 kcal/mol higher than the ground state for a given spin. For example, the ground spin state of CH_2/Pt_8 is $S = 2$, leading to 72 doubly occupied d orbitals and four singly occupied d orbitals. To ensure that this is indeed the ground state, the occupations of the lowest singly occupied d orbital and the highest doubly occupied orbital are switched and the energy is recalculated. If the energy drops, then the switch occurs with the next doubly occupied orbital until the energy no longer decreases. Although not exhaustive, this general procedure gives us reasonable confidence that the calculated energies are indeed the ground states.

The ground spin states and total energies of the six M_8 clusters are given in Table 2. In each case, except Pd, the electronic structure is consistent with the IEM, which suggests s^1d^{N-1} character in the surface, where N is the number of valence electrons. The ground spin states for the metal and metal−adsorbate clusters follow a coherent pattern based on the IEM. Details are provided in earlier papers.[10−12] We ensured in each case that the optimum spin states are used in calculating the bond energies.

6.4. Comparison of Explicit and Implicit Corrections for H/Pt_8. Using our scheme of implictly correcting for zero point energy and enthalpy at room temperature, we calculate $H_f(H/Pt_8) = -11.38$ kcal/mol.[11] Instead we can explicitly compute these quantities.

The calculated non-ZPE corrected QM binding energy of H/Pt_8 is 67.2 kcal/mol. The three modes have frequencies summing to $\sim$2000 cm^{-1}. Hence, the computed zero point energy correction is $\sim$1000 cm^{-1} in energy or 2.9 kcal/mol per H atom. Therefore the ZPE-corrected binding energy of H/Pt_8 is $67.2-2.9 = 64.3$ kcal/mol.

The calculated non-ZPE corrected QM bond strength of H−H is 111.7 kcal/mol. The calculated ZPE is 6.1 kcal/mol. Therefore, the ZPE-corrected bond energy is $111.7 - 6.1 = 105.6$ kcal/mol.

Hence, $H_f(H/Pt_8) = 0.5(105.6 - 2 \times 64.3) = -11.0$ kcal/mol. Enthalpy corrections to room-temperature result in stabilizing the adsorbate by 1.2 kcal/mol. Therefore the final computed number with explicit ZPE and thermal enthalpy corrections is $H_f(H/Pt_8) = -12.2$ kcal/mol. Using our scheme of implicit inclusion gives −11.4 kcal/mol, a difference of only 0.8 kcal/mol.

Acknowledgment. This research was funded by NSF (CHE 95-22179). The facilities of the MSC are also supported by grants from DOE-ASCI, ARO/DURIP, ARO/MURI, BP Chemical, Beckman Institute, Seiko-Epson, Exxon, Owens-Corning, Avery-Dennison, Asahi Chemical, Chevron Petroleum Technology Co., Chevron Chemical Co., and Chevron Research and Technology Corp.

JA993336L